JACS
JOURNAL OF THE AMERICAN CHEMICAL SOCIETY
Article
pubs.acs.org/JACS

Chiral Peropyrene: Synthesis, Structure, and Properties

Wenlong Yang,[†] Giovanna Longhi,[‡] Sergio Abbate,[‡] Andrea Lucotti,[§] Matteo Tommasini,[§] Claudio Villani,[#] Vincent J. Catalano,[†] Aleksandr O. Lykhin,[†] Sergey A. Varganov,[†] and Wesley A. Chalifoux*[,†]

[†]Department of Chemistry, University of Nevada—Reno, Reno, Nevada 89557, United States
[‡]Dipartimento di Medicina Molecolare e Traslazionale, Università di Brescia, Viale Europa 11, 25123 Brescia, Italy
[§]Dipartimento di Chimica, Materiali e Ingegneria Chimica "G. Natta", Politecnico di Milano, Piazza Leonardo da Vinci 32, 20133 Milano, Italy
[#]Dipartimento di Chimica e Tecnologie del Farmaco, Universitá di Roma "La Sapienza", 00185 Roma, Italy

Supporting Information

ABSTRACT: Herein we describe the synthesis, structure, and properties of chiral peropyrenes. Using *p*-terphenyl-2,2″,6,6″-tetrayne derivatives as precursors, chiral peropyrenes were formed after a 4-fold alkyne cyclization reaction promoted by triflic acid. Due to the repulsion of the two aryl substituents within the same bay region, the chiral peropyrene adopts a twisted backbone with an end-to-end twist angle of 28° that was unambiguously confirmed by X-ray crystallographic analysis. The chiral peropyrene products absorb and emit in the green region of the UV−visible spectrum. Circular dichroism spectroscopy shows strong Cotton effects ($\Delta\varepsilon = \pm 100$ M^{-1} cm^{-1} at 300 nm). The Raman data shows the expected D-band along with a split G-band that is due to longitudinal and transversal G modes. This data corresponds well with the simulated Raman spectra of chiral peropyrenes. The chiral peropyrene products also display circularly polarized luminescence. The cyclization reaction mechanism and the enantiomeric composition of the peropyrene products are explained using DFT calculations. The inversion barrier for racemization was determined experimentally to be 29 kcal/mol and is supported by quantum mechanical calculations.

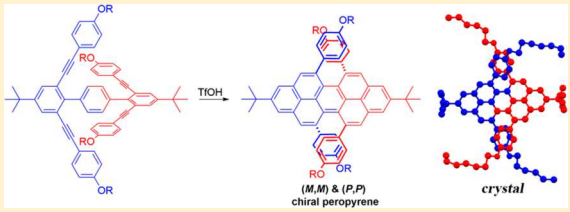

INTRODUCTION

Bottom-up synthetic efforts toward well-defined, nanosized polycyclic aromatic hydrocarbons (PAHs) have captured the attention of chemists for many years because of their interesting optical and electronic properties, making them of interest for a host of applications.[1] Compared to planar PAHs, nonplanar PAHs,[2] such as circulenes,[3] helicenes,[4] and twisted acenes[5] (as shown in Figure 1a), show a variety of fascinating molecular packing and structures due to their curved π-electron system. Helicene-like molecules are an interesting class of nonplanar PAHs that can be defined as ortho-fused PAHs, and the deviation of planarity is a result of intramolecular steric repulsion. Due to their helical structure, some useful properties such as chiroptical, nonplanarity, optical rotation (OR), and dynamic behavior make them of great interest for applications in nonlinear optics, switches, and sensors.[4d,6] Recently, compounds with multihelicity (i.e., more than one helicene within the same molecule) have garnered attention due to their plural electronic states and interesting molecular dynamics.[7]

High racemization barriers lead to persistently chiral PAHs and enable the complete separation of enantiomers. The barrier can be affected by the crowdedness of atoms (from [3]helicene to [5]helicene, Figure 1b) and the bulk of substituents on the same bay regions (H vs Br vs phenyl, Figure 1c).[8] Osswald and Würthner systematically studied the effects of bay substituents on the racemization barriers of perylene bisimides (PBIs) (Figure 1c).[9] Bay-functionalized PBIs can be readily prepared from commercially available perylenetetracarboxylic dianhydride; therefore, their properties and expanded applications could be fully investigaed.[8,10] Compared to PBIs, peropyrene contains a more rigid core backbone. Peropyrene is a flat, planar PAH when unsubstituted on the bay regions. Peropyrene has recently attracted interest as a promising singlet fission material, making derivatives of this compound attractive synthetic targets.[11] Recently, we reported the synthesis of 5,13-disubstituted peropyrenes through the benzannulation reaction of alkynes promoted by triflic acid (TfOH).[12] The steric repulsion of the aryl groups and the hydrogen substituents at the bay positions results in the peropyrene being axially chiral in the solid-state with an end-to-end twist angle of 18°. We envisaged that the peropyrene core would twist even more if we were able to introduce two substituents within the same bay region (Figure 1d). This seemed like a challenging endeavor using our previously reported 4-fold alkyne cyclization methodology,[12,13] as this would ultimately result in both bay regions being doubly substituted. However, we thought that the high-energy alkyne-

Received: July 1, 2017
Published: August 22, 2017

DOI: 10.1021/jacs.7b06848
J. Am. Chem. Soc. 2017, 139, 13102−13109

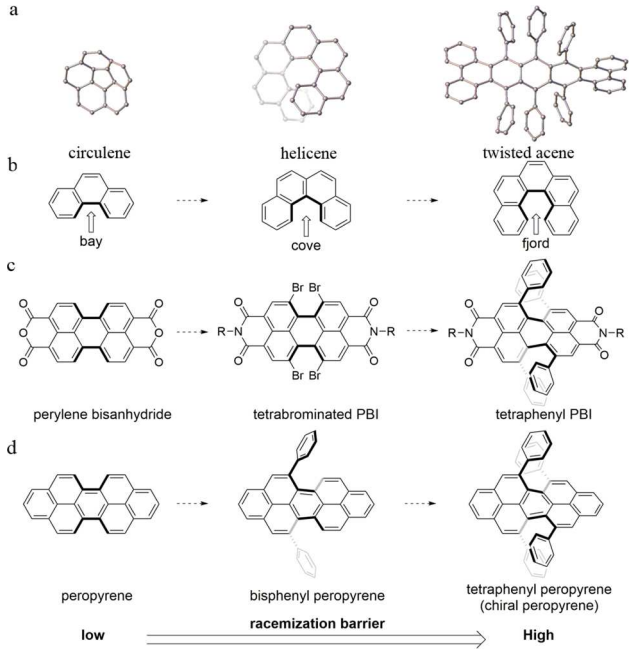

Figure 1. (a) Nonplanar PAHs. (b) [3]Helicene to [5]helicene. (c) Perylene bisanhydride to tetraphenyl PBI. (d) Peropyrene to chiral peropyrene.

containing precursors might provide the thermodynamic driving force to allow us to synthesize these seemingly impossible to make compounds. To the best of our knowledge, a method for the synthesis of a persistently twisted and thus chiral 5,6,12,13-tetrasubstituted peropyrenes has never been reported. Herein, we report the synthesis, characterization, and properties of chiral peropyrenes. The high conformational stability of these compounds enabled their complete enantiomeric separation and characterization. This work not only exhibits a convenient method to introduce rigid and bulky substituents on the bay positions to generate nonplanar PAHs but also introduces new perspectives on the accessibility of nonplanar PAHs with a view toward potential applications in material science.

RESULTS AND DISCUSSION

Design and Synthesis of Chiral Peropyrenes. The benzannulation reaction of alkynes has been shown to proceed with Brønsted acids,[13,14] π-Lewis acids,[15] and other electrophiles.[16] Recently, we have reported the successful synthesis of pyrenes, peropyrenes, and teropyrenes through the benzannulation reaction of alkynes promoted by triflic acid (TfOH).[12a] We also applied this methodology to the bottom-up solution-phase synthesis of graphene nanoribbons.[17] Herein, we demonstrate that this efficient method works well to provide chiral peropyrenes with tremendous steric hindrance within both bay regions of the molecule (Scheme 1). The synthesis of **1** was achieved using methodology we have previously reported, followed by a double Suzuki cross-coupling reaction to afford the key precursors **2a–2d** in modest yields. The modest yields are understandable considering that compounds **2a–2d** are sterically hindered with the ethynylaryl substituents being relatively close in space, as seen in the X-ray crystal structure of **2a** (Scheme 1). With precursors **2a–2d** in hand, the addition of trifluoroacetic acid (TFA) resulted in the clean formation of bis-cyclized products **4a–4d**, which were isolated and fully characterized. Monocyclized products **3a–3d** were not observed at the end of the reaction. What was interesting was that although there were three possible products from a 2-fold alkyne cyclization reaction, only product **4** was observed, where bis-cyclization occurred on the same side of the molecule to make a picene derivative, as seen in the X-ray crystal structure of **4a** (Scheme 1). The other two possible products, **5** and **6**, were not detected. The formation of compound **4** was also supported by NMR spectroscopy. We conducted a computational study of this acid-mediated bis-cyclization reaction that supported the kinetic preference for the syn-cyclization path to afford picene product **4** [Figure S2 and Table S1, Supporting Information (SI)].

According to a previous study,[12b] we knew that TFA was not acidic enough to evoke a 4-fold cyclization, so we turned to stronger acids, such as methanesulfonic acid (MSA) and triflic acid (TfOH). Only a trace amount of chiral peropyrene was observed when using excess MSA (50–100 equiv) at room temperature, with significant amounts of bis-cyclized product still observed in the reaction mixture. Increasing the temperature did not improve the conversion or yield but rather led to significant decomposition. To our delight, chiral peropyrenes **8** were isolated in moderate yield when a solution of bis-cyclized product **4** was slowly transferred to a CH_2Cl_2 solution of TfOH at −40 °C. We also observed a small amount of tricyclized product **7** left at the end of the reaction that was not easily separated by chromatography, except **7a**. Increasing the reaction time or temperature in an attempt to fully convert the tricyclized intermediate **7** to product **8** led to diminished yields. Peropyrenes **8** can possibly exist as three isomers: the (*P*,*P*)- and (*M*,*M*)-enantiomers, as well as the (*P*,*M*)/(*M*,*P*)-meso isomer. However, the results showed that no meso compound could be detected, which is in contrast to what is observed in other chiral syntems.[7a,c,g] This was supported by NMR and high-performance liquid chromatography (HPLC) analysis (vide infra).

Analysis of NMR Spectra. Chiral peropyrene products **8b–8d** are highly soluble in common organic solvents, allowing their characterization by NMR spectroscopy. Broad peaks appeared for the bay region aryl protons in the ^{1}H NMR ($CDCl_3$) spectra of cyclized compound **4b** and **8b**. It should be noted that broadening was not observed in the reported tetraphenyl-substituted PBIs.[10c] This is due to restricted free-rotation of the aryl substituents at room temperature (red circles, Figure 2a) within the newly formed diaryl-substituted bay regions. In the case of bis-cyclized intermediate **4**, the two aryl substituents terminating the ethynyl groups (blue circles, Figure 2a) are still capable of free-rotation, as evidenced by the relatively sharp signals for those aryl protons in the ^{1}H NMR spectrum. The four aryl substituents in compound **8** showed broad peaks in the ^{1}H NMR spectra. Likewise, the ^{13}C NMR spectra of **8** exhibit four significantly broadened signals, which were assigned to the aryl substituents. To prove our hypothesis, compound **8b** was studied by ^{1}H and ^{13}C NMR and ^{1}H–^{13}C correlation NMR (heteronuclear single quantum coherence, HSQC) spectroscopy in $CDCl_3$ at 50 °C [Figures 2b and S13 and S14 (SI)]. We found that, after increasing the temperature to 50 °C, the broad peaks converged to two relatively sharp peaks in the ^{1}H NMR spectrum. This was also observed in the ^{13}C NMR spectrum. Analysis of the HSQC spectrum at 50 °C showed correlations between the broad ^{1}H and ^{13}C peaks, greatly simplifying the structure assignment of **8b**. Furthermore, compound **8b** was studied by variable temperature (VT) ^{1}H

DOI: 10.1021/jacs.7b06848
J. Am. Chem. Soc. 2017, 139, 13102–13109

Scheme 1. Synthesis of Axially Chiral Peropyrenes 8 and Possible Intermediates[a]

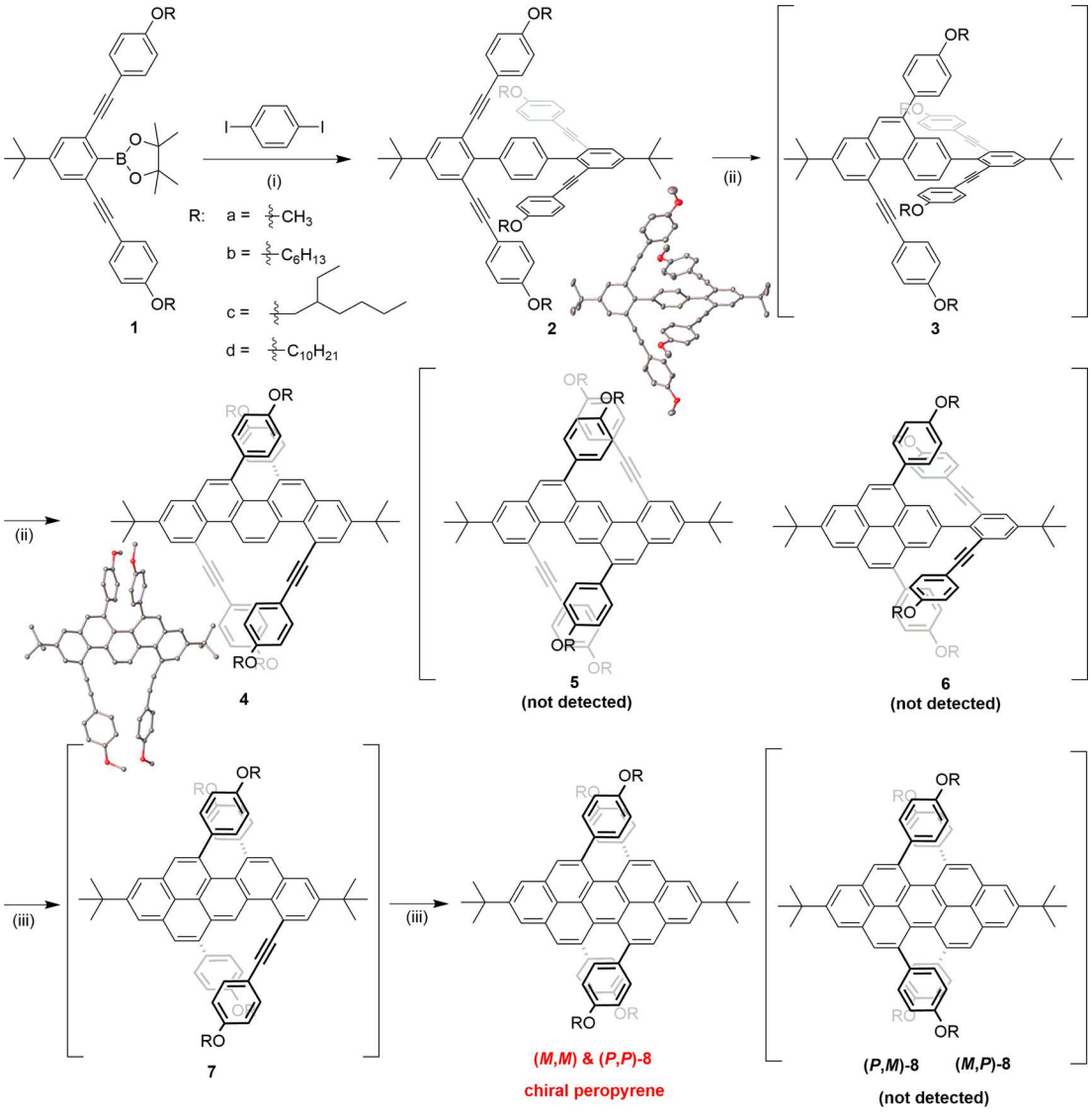

[a]Reaction conditions: (i) **1** (2.2 equiv), 1,4-diiodobenzene (1 mmol), $Pd(PPh_3)_4$ (10 mol %), Ag_2CO_3 (4 equiv), THF, 80 °C, 24 h (**2a**, 42%; **2b**, 39%, **2c**, 47%, **2d**, 44%). (ii) TFA (50 equiv), CH_2Cl_2, rt, 1 h (**4a**, 97%; **4b**, 94%, **4c**, 96%, **4d**, 95%). (iii) TfOH (20 equiv), CH_2Cl_2, −40 °C, 30 min (**8a**, 28%; **8b**, 40%, **8c**, 38%, **8d**, 35%).

NMR spectroscopy in *d*-DMSO between 25 and 100 °C (Figure S15, SI). The broad peaks resulting from the aryl substituents gradually sharpen as a function of increasing temperature, and the signals recover to broad peaks when the sample is cooled back to 25 °C. It should be noted that no obvious decomposition of the sample was observed, even after being dissolved in $C_2D_2Cl_4$ solution for 2 months in an NMR tube.

X-ray Crystallographic Analysis. The structure of chiral peropyrene **8b** was unambiguously confirmed by X-ray crystallographic analysis of a racemic single crystal (Figure 3a). The X-ray crystal structure clearly showed a twisted π-system, which is caused by repulsion (on both sides of the molecule) between the two aryl substituents within the same bay region. The distance between two aryl substituents within the same bay region was only 2.9 Å, and the splay angle of the bay region is ∼29° with an end-to-end twist angle of 28° (Figure 3b). A face-to-face molecular packing was found, with an interplanar spacing of 9 Å (Figure 3b).

Separation, Isomerization, Circular Dichroism, and Optical Rotation. The separation of the enantiomers and their characterization with most recent chiroptical spectroscopies available to-date are presented. The data provides insight into the conformational aspects of chiral peropyrenes, allows the assignment of absolute configuration (AC), and demonstrates their utility in applications such as chiral organic light emitters. Excellent separation of the enantiomers of peropyrene **8b** was achieved by HPLC using a column packed with a chiral stationary phase based on amylose tris(3,5-dimethylphenylcarbamate) immobilized on silica gel.[18] Elution with hexane/2-propanol (98/2 v/v) gave two nicely resolved peaks corresponding to the (*P*,*P*)- and (*M*,*M*)-enantiomers of **8b**, with elution times of 3.2 and 5.2 min, respectively. When monitored by CD detection at 300 nm, bisignate peaks of equal area were observed, as expected for a racemate (Figure 4a). The analytical separation was easily scaled up to the milligram range using a 250 × 10 mm column packed with the same material used in the analytical column. Iterative chromatography with

DOI: 10.1021/jacs.7b06848
J. Am. Chem. Soc. 2017, 139, 13102−13109

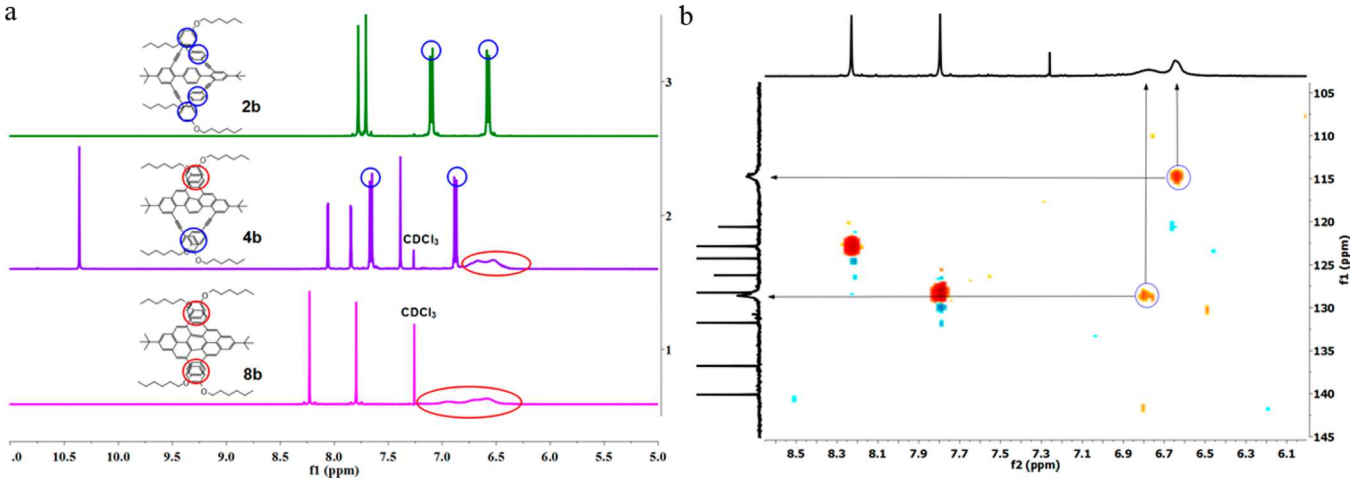

Figure 2. (a) Aromatic region of ^{1}H NMR spectra of compounds **2b**, **4b**, and **8b** in $CDCl_3$ at room temperature. (b) Aromatic region HSQC NMR spectra of compound **8b** in $CDCl_3$ at 50 °C.

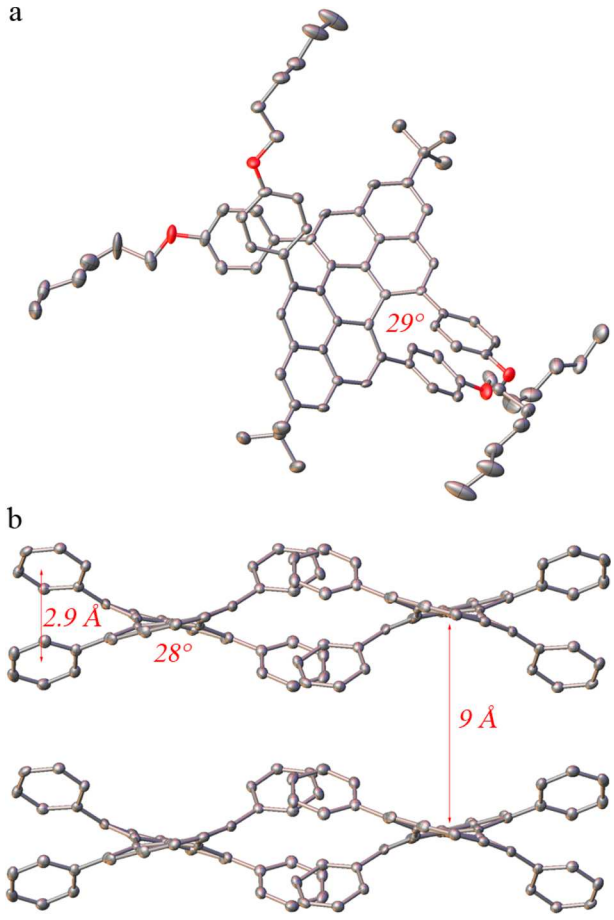

Figure 3. Thermal ellipsoids plot of **8b** (ellipsoids at 50% probability, hydrogens removed for clarity): (a) skewed view and (b) packing arrangements (only the backbone is shown for clarity).

fraction collection and pooling afforded the individual enantiomers of **8b** with ee = 99.9%, $[\alpha]_D$ = +1438 and ee = 97.3%, $[\alpha]_D$ = −1403 for the first- and second-eluted enantiomers, respectively. Thermal racemization of the second-eluted enantiomer of **8b** in decalin at 100 °C was monitored by HPLC following the decay of the enantiomeric excess over time, and a racemization rate constant value k_{rac} = 0.0027 min^{-1} (T = 100 °C) was determined (Figure S1, SI). For the enantiomer interconversion of **8b**, where a stepwise process converts one enantiomer into the unstable meso form and then into the other enantiomer (see the section on the theoretical study), the statistical transmission coefficient f = 0.5 was used in the calculation of the free energy barrier $\Delta G^{\ddagger}$ for a single inversion (*M*,*M* or *P*,*P* to meso) from the rate constant of the overall process.[19] This gave a value of $\Delta G^{\ddagger}$ = 28.9 ± 0.1 kcal/mol at 100 °C and is consistent with the computational study (vide infra).

The optical rotation (OR) value $[\alpha]_{589}^{25}$ = +1438 (c = 8.69 × 10^{-3} g/L in CH_2Cl_2) is quite large and is similar to that observed in other helicene systems.[20] This large OR value is due to the fact that the first absorption and CD features are close in wavelength to where the OR is measured (vide infra), and thus, according to the Kramers−Kronig (KK) relation, results of OR are intensified. This is caused by the inverse difference in square wavelength from the wavelength of electronic transitions.[21] As a consequence, when the OR is measured for smaller wavelengths, anomalous optical rotatory dispersion (ORD)[21] is observed. In the Supporting Information (Figures S3), we provide the KK curve derived from the electronic circular dichroism (ECD) spectra (vide infra), and we have checked that the experimental values for $[\alpha]$ at 589, 577, 436, 405, and 365 nm show excellent agreement with the theoretical KK curve.

Experimental ECD and absorption spectra are given in the Figure 4b,c for both peropyrene (**8b**) enantiomers. A nearly constant g factor ($\Delta\varepsilon/\varepsilon$) of about 1.2 × 10^{-3} is observed for the features detected in the range 460−530 nm: $\Delta\varepsilon = \varepsilon_L - \varepsilon_R$, where ε_L and ε_R are the molar extinction coefficients for left and right circularly polarized light, respectively. The longer wavelength features are vibronic; the same happens in the fluorescence and circularly polarized luminescence (CPL) spectra and is confirmed by quantum mechanical calculations (vide infra). Time-dependent density functional theory (TD-DFT) calculations have been conducted for peropyrene **8b**, where we substituted the four *O*-hexyl groups with four *O*-methyl groups (**8a**) and assumed the (*M*,*M*)-configuration. With the former assumption, we avoided the complication of considering the multiplicity of aliphatic chain conformations, with no prejudice on the chromophoric transitions. As previously reported, when calculating the chiroptical re-

DOI: 10.1021/jacs.7b06848
J. Am. Chem. Soc. 2017, 139, 13102−13109

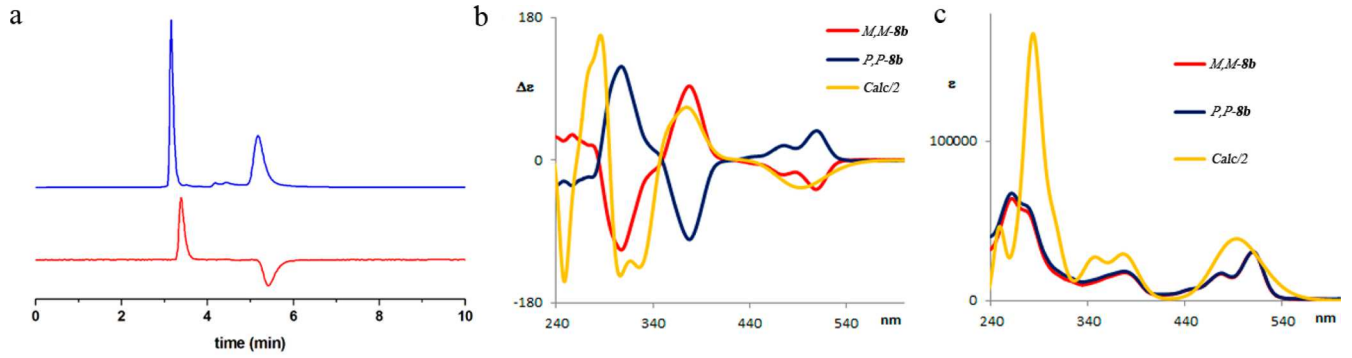

Figure 4. (a) Chiral HPLC traces with UV (blue) and CD (red) detection at 300 nm. Retention times of the two enantiomers are 3.2 and 5.2 min. (b) CD spectra of **8b** (blue, first eluted; red, second eluted) and the calculated CD of the model structure [(*M*,*M*)-enantiomer, yellow]. (c) Absorption spectra of the two enantiomers in CH_2Cl_2 solution and the calculated spectra. (Spectra were calculated at the CAM-B3LYP/6-31G(d,p) level.)

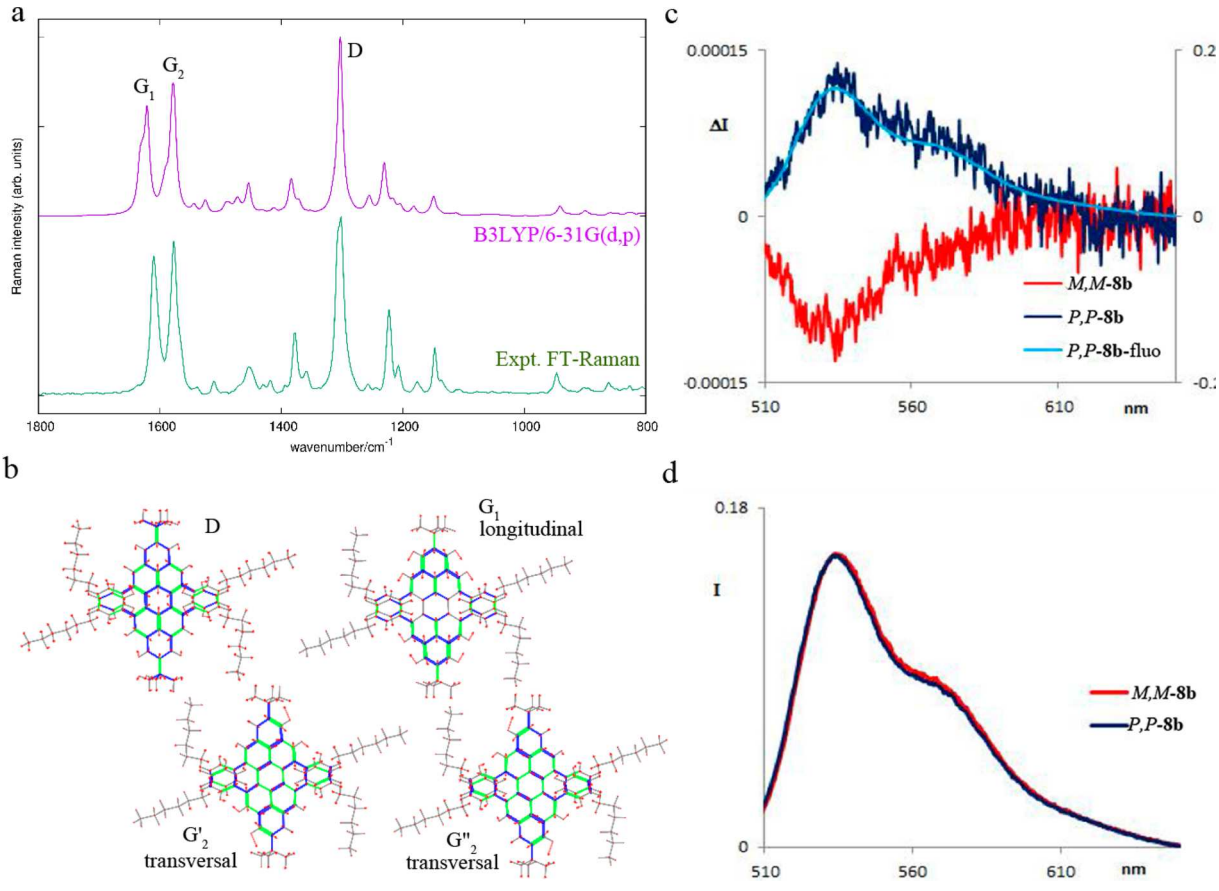

Figure 5. (a) Experimental FT-Raman spectrum of **8b** (1064 nm excitation wavelength) and simulated off-resonance Raman spectrum from DFT calculations [B3LYP/6-31G(d,p), uniformly frequency-scaled by 0.98]. (b) Nuclear displacements of the G and D modes of **8b** computed by DFT: red arrows represent displacement vectors; C−C bonds are represented as green and blue lines of different thicknesses according to their relative stretching (shrinking). (c) CPL spectra of **8b**. (d) Fluorescence spectra of its two enantiomers.

sponse,[22] contributions from different conformers must be taken into account: we checked that the orientation of the *O*-methyl groups has no influence on the peropyrene low-energy electronic transitions and that the phenyl orientation is strictly connected with peropyrene distortion. The following theoretical study of the interconversion confirms that only one structure has appreciable population. This analysis allowed us to obtain the simulated spectrum of (*M*,*M*)-**8b** (Figure 4b), which is superimposed on the experimental spectra. The AC is assigned to the (*M*,*M*)-configuration, which corresponds to the second-eluted enantiomer bearing a negative (−) OR sign at 589 nm. This is what is observed for helicene systems, namely, [5], [6], [7], or even higher-membered helicenes.[20,23] To complete the discussion of the observed CD spectra, one may notice that a similar chiroptical response is encountered in perylene bisimides.[24] In particular, the lowest energy transition is characterized by electric and magnetic transition moments that are both parallel to the long axis of the peropyrene moiety. The second observed feature of opposite sign can be associated with two transitions with transition dipole moments parallel to

DOI: 10.1021/jacs.7b06848
J. Am. Chem. Soc. 2017, 139, 13102−13109

the transverse axis. In both cases, the electric and magnetic dipole transition moments are parallel (or antiparallel), so the calculated sign can be considered correct. The characteristics of the lowest energy transition are maintained in the excited state, giving an analogous description of the CPL band. Transition moments and assignments are reported in Table S3 (SI).

Raman, Fluorescence, and Circularly Polarized Luminescence. Raman spectroscopy is often used to investigate the spectroscopic and structural properties of highly π-conjugated molecular systems. The experimental FT-Raman spectrum of the racemic powder of sample **8b** is reported in Figure 5a and compared with results from DFT calculations. The expected G and D Raman features of graphene molecules[1] clearly emerge, and the associated nuclear displacement patterns nicely match those previously observed in another chiral polycyclic aromatic hydrocarbon (2-Br-hexahelicene[23a]) or in the nonplanar perchlorinated hexa-*peri*-hexabenzocoronene.[25] In addition to perchlorinated hexa-*peri*-hexabenzocoronene and 2-Br-hexahelicene, the present case of **8b** clearly supports the observation that the nonplanarity of these molecules is not hindering the formation of the typical collective Raman modes associated with the graphene cores. This can be taken as the hallmark of π-conjugation, which in these systems is just modulated by nonplanarity and not seriously weakened.

Interestingly, because compound **8b** has lower symmetry than graphene, the E_{2g} degeneracy of the G peak is lifted. Hence, longitudinal and transversal G modes are found, which also explains the split G feature observed in the FT-Raman spectrum. On the other hand, the D peak has a very distinct vibrational pattern and it shows up as the strongest Raman line (Figure 5a). The simulated and observed Raman spectrum showed good correspondence. Finally, we anticipate that the analysis of the vibrational modes will be useful for the interpretation of fluorescence and circularly polarized luminescence (CPL) data presented below.

Next we investigated the fluorescence properties of peropyrene **8b**, studying the CPL with a home-built apparatus.[26] The results showed that the CPL (Figure 5c) is weak; however, the fluorescence is very intense (Figure 5d). The g(luminescence) factor, $(\Delta I/I) \approx 7.7 \times 10^{-4}$ {with $I = [(I_L + I_R)/2]$ being the total intensity of emitted light and $\Delta I = I_L - I_R$, with I_L and I_R being the left and right circularly polarized components of emitted radiation}, is slightly smaller than the g factor for absorption (vide supra). The observed Stokes shift is quite low and evident vibronic structuring is observed; the latter interpretation is also backed by the computations commented below. As in most CPL studies, the sign of the single CPL feature is the same as the sign of the longest wavelength ECD band. For helicene systems,[27] two situations are met: one in which the CPL features are sensitive to substituents and the other in which CPL is promoted only by intrinsic helicity. In the former case, CPL is weak; with rotational strengths being very weak, vibronic effects dominate and dictate the observed sign.[27b,28] In the latter case (see, for example, ref 28a), the CPL is strong due to the presence of heteroatoms within the helical structure, while vibronic effects are almost negligible. In the present case, the intensities of the low-energy absorption/CD bands and emission/CPL signals are quite large. The calculated dipole and rotational strengths are similar in the ground and excited states, coherently with very similar geometries for ground and excited states and small Stokes shift (see Figure S4 and Tables S4 and S5, SI): the g factors are low in both absorption and emission, since the dipole strengths are very large.

The observation that the g-factor is constant throughout the vibronic structures suggests that Franck–Condon terms dominate.[28] This greatly simplifies vibronic calculations, and indeed, the vibronic structure relative to the absorption/emission related with the lowest lying bright excited state of **8b** can be accounted for with a straightforward approach, where the Huang–Rhys (HR) factors are computed with TD-DFT methods and used to determine the relative intensities over the manifold of vibronic transitions (see the SI, general experimental section). Despite the basic displaced harmonic oscillator approximation, certainly less accurate than other treatments including the effects of Dushinsky rotation,[29] this kind of theoretical approach reasonably accounts for the observed line shapes. Even more interesting, among the six modes with sizable HR factors (Table 1), we find those

Table 1. List of HR Factors Considered in the Calculation of the Vibronic Line Shape According to TD-CAM-B3LYP/6-31G(d,p) Calculations (see the SI for details about the assignment of the modes)

wavenumber (cm^{-1})	HR factor	mode
108.8	0.1887	molecular torsion
147.2	0.5581	tearing mode
189.6	0.4194	transversal stretching
559.0	0.1556	*t*-Bu umbrella
1351.3	0.1801	D line (mode 1)
1360.8	0.1369	D line (mode 2)

associated with the Raman G and D lines and several observed low wavenumber modes (see the SI, section 3.5). This establishes a connection between the characterization of the vibrational structure and the electronic spectroscopy of the S_1 state of **8b**. Results for absorption and emission are reported in Figure S5 and summarized in Table S6 (SI). In the Supporting Information we also report a picture comparing the ground and excited state geometries (followed by a table with bond length values, Table S5); this picture strongly resembles structures of the normal modes reported in Figure 5b, suggesting the role of the D mode in determining the spacing between the observed transitions along the vibronic structure. On the other hand, the low wavenumber modes, bearing sizable Huang–Rhys factors, contribute the most in determining the effective line width of the vibronic structure (see Table S7 and associated discussion, SI). These modes can be described as collective deformations of the molecule as a whole, and some of them resemble other cases investigated in the past, notably the longitudinal and transversal acoustic-like stretching of the molecule.[30] Additional modes characteristic of **8b** include the umbrella of the *t*-Bu groups and the torsion mode of the aromatic core.

Theoretical Study of the Interconversion. As expected, the computational study confirms that the inversion between enantiomers (*M*,*M*)-**8a** and (*P*,*P*)-**8a** proceeds through the achiral intermediate *meso*-**8a**, lying 10.0 kcal/mol above the enantiomers **8a**, through transition states with an activation energy of 29.2 kcal/mol [Figure 6 and Table S2 (SI)]. The inversion can be explained by a two-step mechanism in which a face-to-face rotation of two methoxyphenyls initially takes place on the one side of the molecule to arrive at the transition state (TS_1/TS_2), and then this is repeated on the opposite side of the molecule to arrive at the enantiomer. The simultaneous

DOI: 10.1021/jacs.7b06848
J. Am. Chem. Soc. 2017, 139, 13102–13109

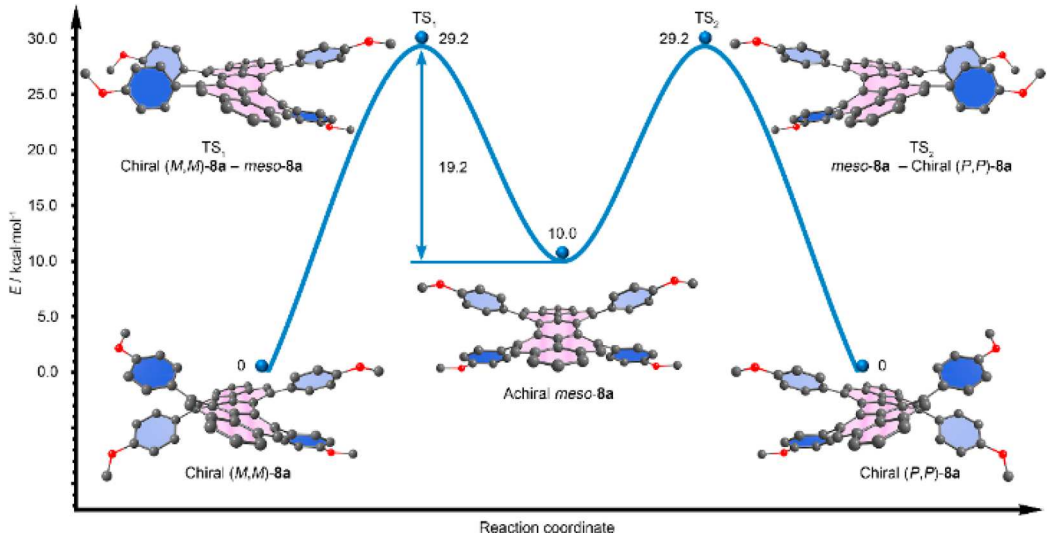

Figure 6. Reaction path of peropyrene inversion connecting the enantiomers (*M*,*M*)-**8a** and (*P*,*P*)-**8a** via the intermediate achiral compound *meso*-**8a** (*tert*-butyl groups were omitted). See the SI for details about the level of theory used.

rotation of all four methoxyphenyls corresponds to a very high energy path without an intermediate, which is unlikely to be relevant to the inversion of chirality. In the meantime, using the experimental free energy barrier for the (*M*,*M*) to (*P*,*P*) interconversion $\Delta G^{\neq} \sim 29$ kcal/mol, we can calculate a half-life time for the individual enantiomers to be $t_{1/2} \sim 2$ h at $T = 100$ °C.

CONCLUSION

In summary, the first axially chiral peropyrenes were successfully prepared through a Brønsted acid promoted 4-fold alkyne benzannulation strategy. The twisted structure was unambiguously confirmed by X-ray crystallography, showing two helicene-like moieties within the two bay regions. The high racemization energy barrier enabled the separation of the two isomers, which were carefully investigated. In addition, the whole process of the reaction was also studied computationally. We believe that this new synthetic strategy here would allow us to rapidly construct a variety of new and fascinating chiral PAHs.

ASSOCIATED CONTENT

Supporting Information

The Supporting Information is available free of charge on the ACS Publications website at DOI: 10.1021/jacs.7b06848.

Experimental procedures, NMR spectra, supplementary X-ray crystallographic analysis, and computational study (PDF)

Crystal data in cif format for **2a** (CIF)

Crystal data in cif format for **4a** (CIF)

Crystal data in cif format for **8b** (CIF)

AUTHOR INFORMATION

Corresponding Author

*wchalifoux@unr.edu

ORCID

Wenlong Yang: 0000-0002-9017-7728

Giovanna Longhi: 0000-0002-0011-5946

Sergio Abbate: 0000-0001-9359-1214

Matteo Tommasini: 0000-0002-7917-426X

Claudio Villani: 0000-0002-3253-3608

Aleksandr O. Lykhin: 0000-0002-9366-5866

Wesley A. Chalifoux: 0000-0002-6849-6829

Notes

The authors declare no competing financial interest.

ACKNOWLEDGMENTS

W.A.C. acknowledges the Donors of the American Chemical Society Petroleum Research Fund for partial financial support of this research (PRF No. 53543-DNI1). W.A.C. also thanks the University of Nevada—Reno, for startup funds and the National Science Foundation (NSF) for partial financial support through a CAREER Award (CHE-1555218). S.A.V. thanks the University of Nevada—Reno, for startup funds and the NSF for financial support through a CAREER Award (CHE-1654547). A.O.L. thanks the RFBR, Government of Krasnoyarsk Territory, and Krasnoyarsk Region Science and Technology Support Fund for the grant No. 16-43-243052. We thank Dr. Jorge H. S. K. Monteiro for his assistance with the quantum yield measurements.

REFERENCES

(1) (a) Wöhrle, T.; Wurzbach, I.; Kirres, J.; Kostidou, A.; Kapernaum, N.; Litterscheidt, J.; Haenle, J. C.; Staffeld, P.; Baro, A.; Giesselmann, F.; Laschat, S. *Chem. Rev.* **2016**, *116*, 1139. (b) Narita, A.; Wang, X.-Y.; Feng, X.; Müllen, K. *Chem. Soc. Rev.* **2015**, *44*, 6616. (c) Narita, A.; Feng, X.; Müllen, K. *Chem. Rec.* **2015**, *15*, 295. (d) Ball, M.; Zhong, Y.; Wu, Y.; Schenck, C.; Ng, F.; Steigerwald, M.; Xiao, S.; Nuckolls, C. *Acc. Chem. Res.* **2015**, *48*, 267. (e) Sun, Z.; Zeng, Z.; Wu, J. *Acc. Chem. Res.* **2014**, *47*, 2582. (f) Kawasumi, K.; Zhang, Q.; Segawa, Y.; Scott, L. T.; Itami, K. *Nat. Chem.* **2013**, *5*, 739. (g) Wu, J.; Pisula, W.; Müllen, K. *Chem. Rev.* **2007**, *107*, 718.

(2) (a) Rieger, R.; Müllen, K. *J. Phys. Org. Chem.* **2010**, *23*, 315. (b) Merner, B. L.; Dawe, L. N.; Bodwell, G. J. *Angew. Chem., Int. Ed.* **2009**, *48*, 5487.

(3) (a) Sakamoto, Y.; Suzuki, T. *J. Am. Chem. Soc.* **2013**, *135*, 14074. (b) Feng, C.-N.; Kuo, M.-Y.; Wu, Y.-T. *Angew. Chem., Int. Ed.* **2013**, *52*, 7791. (c) Bharat; Bally, T.; Valente, A.; Cyrański, M. K.; Dobrzycki, Ł.; Spain, S. M.; Rempała, P.; Chin, M. R.; King, B. T.; Bhola, R. *Angew. Chem., Int. Ed.* **2010**, *49*, 399. (d) Tsefrikas, V. M.; Scott, L. T. *Chem. Rev.* **2006**, *106*, 4868. (e) Wu, Y.-T.; Siegel, J. S.

DOI: 10.1021/jacs.7b06848
J. Am. Chem. Soc. 2017, 139, 13102−13109

Chem. Rev. **2006**, *106*, 4843. (f) Sygula, A.; Rabideau, P. W. *J. Am. Chem. Soc.* **2000**, *122*, 6323. (g) Yamamoto, K.; Harada, T.; Okamoto, Y.; Chikamatsu, H.; Nakazaki, M.; Kai, Y.; Nakao, T.; Tanaka, M.; Harada, S.; Kasai, N. *J. Am. Chem. Soc.* **1988**, *110*, 3578. (h) Barth, W. E.; Lawton, R. G. *J. Am. Chem. Soc.* **1966**, *88*, 380.

(4) (a) Gingras, M. *Chem. Soc. Rev.* **2013**, *42*, 968. (b) Gingras, M.; Felix, G.; Peresutti, R. *Chem. Soc. Rev.* **2013**, *42*, 1007. (c) Gingras, M. *Chem. Soc. Rev.* **2013**, *42*, 1051. (d) Shen, Y.; Chen, C.-F. *Chem. Rev.* **2012**, *112*, 1463. (e) Rajca, A.; Miyasaka, M.; Pink, M.; Wang, H.; Rajca, S. *J. Am. Chem. Soc.* **2004**, *126*, 15211. (f) Mori, K.; Murase, T.; Fujita, M. *Angew. Chem., Int. Ed.* **2015**, *54*, 6847.

(5) (a) Wang, K. K. Twisted Arenes. In *Polyarenes I*; Siegel, J. S., Wu, Y.-T., Eds.; Springer: Berlin, 2014; p 31. (b) Pradhan, A.; Dechambenoit, P.; Bock, H.; Durola, F. *J. Org. Chem.* **2013**, *78*, 2266. (c) Pascal, R. A. *Chem. Rev.* **2006**, *106*, 4809. (d) Lu, J.; Ho, D. M.; Vogelaar, N. J.; Kraml, C. M.; Pascal, R. A. *J. Am. Chem. Soc.* **2004**, *126*, 11168. (e) Qiao, X.; Ho, D. M.; Pascal, R. A. *Angew. Chem., Int. Ed. Engl.* **1997**, *36*, 1531. (f) Qiao, X.; Padula, M. A.; Ho, D. M.; Vogelaar, N. J.; Schutt, C. E.; Pascal, R. A. *J. Am. Chem. Soc.* **1996**, *118*, 741. (g) Pascal, R. A.; McMillan, W. D.; Van Engen, D.; Eason, R. G. *J. Am. Chem. Soc.* **1987**, *109*, 4660.

(6) (a) Martin, R. H. *Angew. Chem., Int. Ed. Engl.* **1974**, *13*, 649. (b) Katz, T. J. *Angew. Chem., Int. Ed.* **2000**, *39*, 1921. (c) Urbano, A. *Angew. Chem., Int. Ed.* **2003**, *42*, 3986. (d) Daigle, M.; Miao, D.; Lucotti, A.; Tommasini, M.; Morin, J.-F. *Angew. Chem., Int. Ed.* **2017**, *56*, 6213.

(7) (a) Fujikawa, T.; Segawa, Y.; Itami, K. *J. Am. Chem. Soc.* **2016**, *138*, 3587. (b) Kashihara, H.; Asada, T.; Kamikawa, K. *Chem. - Eur. J.* **2015**, *21*, 6523. (c) Fujikawa, T.; Segawa, Y.; Itami, K. *J. Am. Chem. Soc.* **2015**, *137*, 7763. (d) Cheung, K. Y.; Xu, X.; Miao, Q. *J. Am. Chem. Soc.* **2015**, *137*, 3910. (e) Zhong, Y.; Kumar, B.; Oh, S.; Trinh, M. T.; Wu, Y.; Elbert, K.; Li, P.; Zhu, X.; Xiao, S.; Ng, F.; Steigerwald, M. L.; Nuckolls, C. *J. Am. Chem. Soc.* **2014**, *136*, 8122. (f) Bheemireddy, S. R.; Hautzinger, M. P.; Li, T.; Lee, B.; Plunkett, K. N. *J. Am. Chem. Soc.* **2017**, *139*, 5801. (g) Hu, Y.; Wang, X.-Y.; Peng, P.-X.; Wang, X.-C.; Cao, X.-Y.; Feng, X.; Müllen, K.; Narita, A. *Angew. Chem., Int. Ed.* **2017**, *56*, 3374.

(8) Pagoaga, B.; Giraudet, L.; Hoffmann, N. *Eur. J. Org. Chem.* **2014**, *2014*, 5178.

(9) Osswald, P.; Würthner, F. *J. Am. Chem. Soc.* **2007**, *129*, 14319.

(10) (a) Würthner, F.; Saha-Möller, C. R.; Fimmel, B.; Ogi, S.; Leowanawat, P.; Schmidt, D. *Chem. Rev.* **2016**, *116*, 962. (b) Queste, M.; Cadiou, C.; Pagoaga, B.; Giraudet, L.; Hoffmann, N. *New J. Chem.* **2010**, *34*, 2537. (c) Qiu, W.; Chen, S.; Sun, X.; Liu, Y.; Zhu, D. *Org. Lett.* **2006**, *8*, 867. (d) Würthner, F. *Chem. Commun.* **2004**, 1564.

(11) Nichols, V. M.; Rodriguez, M. T.; Piland, G. B.; Tham, F.; Nesterov, V. N.; Youngblood, W. J.; Bardeen, C. J. *J. Phys. Chem. C* **2013**, *117*, 16802.

(12) (a) Yang, W.; Monteiro, J. H. S. K.; de Bettencourt-Dias, A.; Chalifoux, W. A. *Can. J. Chem.* **2017**, *95*, 341. (b) Yang, W.; Monteiro, J. H. S. K.; de Bettencourt-Dias, A.; Catalano, V. J.; Chalifoux, W. A. *Angew. Chem., Int. Ed.* **2016**, *55*, 10427.

(13) Yang, W.; Chalifoux, W. A. *Synlett* **2017**, *28*, 625.

(14) (a) Goldfinger, M. B.; Crawford, K. B.; Swager, T. M. *J. Am. Chem. Soc.* **1997**, *119*, 4578. (b) Goldfinger, M. B.; Swager, T. M. *J. Am. Chem. Soc.* **1994**, *116*, 7895.

(15) (a) Thomson, P. F.; Parrish, D.; Pradhan, P.; Lakshman, M. K. *J. Org. Chem.* **2015**, *80*, 7435. (b) Chen, T. A.; Lee, T. J.; Lin, M. Y.; Sohel, S. M.; Diau, E. W.; Lush, S. F.; Liu, R. S. *Chem. - Eur. J.* **2010**, *16*, 1826. (c) Mamane, V.; Hannen, P.; Furstner, A. *Chem. - Eur. J.* **2004**, *10*, 4556. (d) Fürstner, A.; Mamane, V. *J. Org. Chem.* **2002**, *67*, 6264.

(16) Yao, T.; Campo, M. A.; Larock, R. C. *J. Org. Chem.* **2005**, *70*, 3511.

(17) Yang, W.; Lucotti, A.; Tommasini, M.; Chalifoux, W. A. *J. Am. Chem. Soc.* **2016**, *138*, 9137.

(18) Franco, P.; Zhang, T. *J. Chromatogr. B: Anal. Technol. Biomed. Life Sci.* **2008**, *875*, 48.

(19) (a) Anderson, J. E.; Lehn, J. M. *J. Am. Chem. Soc.* **1967**, *89*, 81. (b) Ceccacci, F.; Mancini, G.; Mencarelli, P.; Villani, C. *Tetrahedron: Asymmetry* **2003**, *14*, 3117.

(20) Abbate, S.; Lebon, F.; Longhi, G.; Fontana, F.; Caronna, T.; Lightner, D. A. *Phys. Chem. Chem. Phys.* **2009**, *11*, 9039.

(21) (a) Moscowitz, A. Theoretical Aspects of Optical Activity Part One: Small Molecules. In *Advances in Chemical Physics*; John Wiley & Sons, Inc.: 2007; Vol. *IV*, pp 67 10.1002/9780470143506.ch2. (b) Polavarapu, P. L.; Petrovic, A. G.; Zhang, P. *Chirality* **2006**, *18*, 723.

(22) Bringmann, G.; Bruhn, T.; Maksimenka, K.; Hemberger, Y. *Eur. J. Org. Chem.* **2009**, *2009*, 2717.

(23) (a) Johannessen, C.; Blanch, E. W.; Villani, C.; Abbate, S.; Longhi, G.; Agarwal, N. R.; Tommasini, M.; Lightner, D. A. *J. Phys. Chem. B* **2013**, *117*, 2221. (b) Lebon, F.; Longhi, G.; Gangemi, F.; Abbate, S.; Priess, J.; Juza, M.; Bazzini, C.; Caronna, T.; Mele, A. *J. Phys. Chem. A* **2004**, *108*, 11752. (c) Burgi, T.; Urakawa, A.; Behzadi, B.; Ernst, K.-H.; Baiker, A. *New J. Chem.* **2004**, *28*, 332. (d) Caronna, T.; Sinisi, R.; Catellani, M.; Luzzati, S.; Abbate, S.; Longhi, G. *Synth. Met.* **2001**, *119*, 79.

(24) (a) Abbate, S.; Lebon, F.; Longhi, G.; Passarello, M.; Turco Liveri, V. *Chirality* **2011**, *23*, 910. (b) Osswald, P.; Reichert, M.; Bringmann, G.; Würthner, F. *J. Org. Chem.* **2007**, *72*, 3403.

(25) Maghsoumi, A.; Narita, A.; Dong, R.; Feng, X.; Castiglioni, C.; Müllen, K.; Tommasini, M. *Phys. Chem. Chem. Phys.* **2016**, *18*, 11869.

(26) Castiglioni, E.; Abbate, S.; Longhi, G. *Appl. Spectrosc.* **2010**, *64*, 1416.

(27) (a) Longhi, G.; Castiglioni, E.; Villani, C.; Sabia, R.; Menichetti, S.; Viglianisi, C.; Devlin, F.; Abbate, S. *J. Photochem. Photobiol., A* **2016**, *331*, 138. (b) Abbate, S.; Longhi, G.; Lebon, F.; Castiglioni, E.; Superchi, S.; Pisani, L.; Fontana, F.; Torricelli, F.; Caronna, T.; Villani, C.; Sabia, R.; Tommasini, M.; Lucotti, A.; Mendola, D.; Mele, A.; Lightner, D. A. *J. Phys. Chem. C* **2014**, *118*, 1682.

(28) Liu, Y.; Cerezo, J.; Mazzeo, G.; Lin, N.; Zhao, X.; Longhi, G.; Abbate, S.; Santoro, F. *J. Chem. Theory Comput.* **2016**, *12*, 2799.

(29) Santoro, F.; Lami, A.; Improta, R.; Bloino, J.; Barone, V. *J. Chem. Phys.* **2008**, *128*, 224311.

(30) Di Donato, E.; Tommasini, M.; Fustella, G.; Brambilla, L.; Castiglioni, C.; Zerbi, G.; Simpson, C. D.; Müllen, K.; Negri, F. *Chem. Phys.* **2004**, *301*, 81.

DOI: 10.1021/jacs.7b06848
J. Am. Chem. Soc. 2017, 139, 13102−13109